

Equilibrium Climate Sensitivity and Transient Climate Response biased low in historical simulations of CMIP6 models

Yue Dong¹, Kyle C. Armour^{1,2}, Cristian Proistosescu³, Timothy Andrews⁴,
David S. Battisti¹, Piers M. Forster⁵, David Paynter⁶, Christopher J. Smith⁵,
Hideo Shiogama⁷

¹Department of Atmospheric Sciences, University of Washington, Seattle, WA, USA

²School of Oceanography, University of Washington, Seattle, WA, USA

³Department of Atmospheric Sciences and Department of Geology, University of Illinois at
Urbana-Champaign, IL, USA

⁴Met Office Hadley Centre, Exeter, UK

⁵School of Earth and Environment, University of Leeds, UK

⁶NOAA/Geophysical Fluid Dynamics Laboratory, Princeton University, Princeton, NJ, USA

⁷National Institute for Environmental Studies, Tsukuba, Japan

Key Points:

- Within CMIP6 models, historical energy budget constraints underestimate equilibrium climate sensitivity and transient climate response
- Atmosphere-only models forced by observed surface warming patterns produce lower values, in line with historical observations.
- Discrepancies between modeled and observed historical surface warming patterns account for the differences in feedbacks and climate sensitivity estimates

Abstract

This study assesses the effective climate sensitivity (EffCS) and transient climate response (TCR) derived from global energy budget constraints within historical simulations of 8 CMIP6 global climate models (GCMs). These calculations are enabled by use of the Radiative Forcing Model Intercomparison Project (RFMIP) simulations, which permit accurate quantification of the historical effective radiative forcing. We find that long-term historical energy budget constraints generally underestimate EffCS from CO₂ quadrupling and TCR from CO₂ ramping, both by 12%, owing to changes in radiative feedbacks and changes in ocean heat uptake efficiency. Atmospheric GCMs forced by observed warming patterns produce lower values of EffCS that are more in line with those inferred from observed historical energy budget constraints. Understanding the discrepancies between modeled and observed historical surface warming patterns remains critical for constraining EffCS and TCR from the historical record.

Plain Language Summary

Here we use climate models to evaluate the extent to which future warming can be inferred from observations of historical warming. To do so, we employ the RFMIP simulations of 8 models to calculate the historical radiative forcing, and assess historical energy budget constraints on two metrics of global warming: effective climate sensitivity and transient climate response. We find that model historical simulations generally underestimate the climate sensitivity and transient climate response, because historical warming patterns differ from projected warming patterns. Simulations with atmosphere-only models using observed warming patterns produce even lower values of climate sensitivity, suggesting that estimates of climate sensitivity based on recent observations may be similarly biased low.

1 Introduction

Equilibrium climate sensitivity (ECS) and transient climate response (TCR) are two fundamental metrics for evaluating climate change projections. ECS represents the *equilibrium* surface warming in response to a doubling of atmospheric CO₂ concentration relative to pre-industrial levels. Although idealized, ECS has been found to explain most of the spread in projected 21st century global temperature change under realistic emission scenarios (Große et al., 2018; Sherwood et al., 2020). TCR represents the *tran-*

53 *sient* surface warming at the time of CO₂ doubling under an idealized 1% per year CO₂
 54 increase. As a measure of transient response, TCR is better constrained and is also in-
 55 formative about the projected degree of global warming in the coming century.

56 In principle, ECS and TCR can be inferred from the global energy balance frame-
 57 work (Gregory et al., 2002):

$$\Delta N = \Delta F + \lambda \Delta T, \quad (1)$$

58 where ΔN is the global-mean top-of-atmosphere (TOA) radiation anomaly (approximately
 59 equal to ocean heat uptake), ΔF is the effective radiative forcing (ERF; Myhre et al.,
 60 2013), ΔT is the global-mean surface air temperature anomaly, and λ is the radiative
 61 feedback parameter (negative for a stable climate). ECS is inferred as: $ECS = -F_{2x}/\lambda_{eq}$,
 62 where F_{2x} is the ERF from CO₂ doubling, and λ_{eq} is the radiative feedback when a new
 63 equilibrium is reached ($\Delta N = 0$). Ideally, ECS can be estimated from equilibrium states
 64 within global climate models (GCM) forced by an abrupt CO₂ doubling (*abrupt2xCO2*)
 65 or CO₂ quadrupling (*abrupt4xCO2*), after sufficiently long integration (Rugenstein et al.,
 66 2020). In practice, ECS is often extrapolated from a linear regression of ΔN against ΔT
 67 for the first 150yrs of *abrupt4xCO2* simulations (Gregory et al., 2004). This extrapola-
 68 tion generally underestimates the true ECS due to changes in radiative feedbacks as cli-
 69 mate equilibrates (Rugenstein et al., 2020), owing to time-evolving surface warming pat-
 70 terns (e.g., Armour et al., 2013; Andrews et al., 2015; Dong et al., 2020), and nonlinear
 71 mean-state dependence of radiative feedbacks (e.g., Caballero & Huber, 2013; Bloch-Johnson
 72 et al., 2015, 2021). Therefore, we refer the ECS values estimated from these non-equilibrium
 73 states to as an *effective* climate sensitivity (EffCS; Andrews et al., 2015; Sherwood et
 74 al., 2020):

$$EffCS = -\frac{F_{2x}}{\lambda_{eff}}, \quad (2)$$

75 assuming the effective radiative feedback (λ_{eff}) at a transient state would remain con-
 76 stant to equilibrium. Specifically, in this paper we denote EffCS values from *abrupt4xCO2*
 77 simulations (through regressions of annual-mean ΔN against ΔT for the first 150yrs)
 78 as $EffCS_{4xCO2}$ (data from Zelinka et al., 2020). We also estimate EffCS values from the
 79 historical energy budget constraints (using Eqs. 1 and 2), in which case we refer to it
 80 as $EffCS_{his}$.

81 For TCR, it is commonly calculated as the global-mean surface air temperature change
 82 averaged over a 20-year period centered on year 70 of the *1pctCO2* simulations where

CO₂ concentration is doubled (denoted here as TCR_{1pct}). The values of TCR can also be estimated from historical energy budget constraints (see more details in Section 4), in which case we will refer to it as TCR_{his}.

EffCS_{4xCO2} and TCR_{1pct} estimates from fully-coupled atmosphere-ocean GCMs (AOGCMs) have been found to be substantially higher than values of EffCS_{his} and TCR_{his} from observed energy budget constraints (e.g., Otto et al., 2013; Lewis & Curry, 2015, 2018; Forster, 2016), raising a key question of whether the AOGCMs are overly sensitive. However, lower values of EffCS_{his} and TCR_{his} have also been found in AOGCM *historical* simulations, but only in a few models (Winton et al. 2020 for GFDL-CM4; Andrews et al. 2019 for HadGEM3-GC3.1-LL; Dessler et al. 2018 for MPI-ESM1.1). The limited number of model studies reflects the fact that the time-varying historical ERF (ΔF in Eq. 1) is not often diagnosed, precluding accurate calculation of radiative feedback and thus EffCS_{his} and TCR_{his}. Some other studies have instead used *abrupt4xCO2* or *1pctCO2* simulations as a surrogate for historical warming (Armour, 2017; Proistosescu & Huybers, 2017; Lewis & Curry, 2018; Dong et al., 2020), or used a rough estimate of historical ERF taken from IPCC AR5 (Myhre et al., 2013) for CMIP5 AOGCMs (Marvel et al., 2018; Gregory et al., 2020). These approaches provide inter-model comparisons, and generally find that EffCS_{4xCO2} is larger than EffCS_{his}, but it is unclear how accurate their estimates are given that they do not use model-specific estimates of ERF (or in some cases lack historical non-CO₂ forcings altogether).

This work is thus motivated by two key questions: (1) how robust is the finding that values of EffCS_{4xCO2} and TCR_{1pct} are higher than values of EffCS_{his} and TCR_{his} estimated using historical energy budget constraints? (2) How do the estimates of EffCS_{his} and TCR_{his} from models compare to those from observed energy budget constraints? The answers to these questions have major implications for how the historical record informs future climate projections. Here we employ simulations of the Radiative Forcing Model Intercomparison Project (RFMIP; Pincus et al., 2016), which provide the time series of historical ERF for 8 CMIP6 AOGCMs (section 2). With ERF in hand, we assess EffCS_{his} and TCR_{his} values within *historical* simulations and compare to the values of EffCS_{4xCO2} and TCR_{1pct} for each of these models (section 3 and 4). We then compare EffCS and TCR estimates between models and observations, and discuss implications for observation-based historical energy budget constraints on EffCS and TCR (section 5).

2 Data

2.1 Historical Effective Radiative Forcing from RFMIP Simulations

The ERF includes rapid adjustments from the atmosphere in response to changes in CO₂ or other forcing agents (Myhre et al., 2013). It can be quantified from the TOA radiation changes within atmosphere-only GCM (AGCM) simulations wherein forcing agents are changed while SST and sea-ice concentration (SIC) fields are fixed at pre-industrial values (Forster et al., 2016). Here we make use of the fixed-SST simulations of RFMIP that are currently available for 8 CMIP6 models (CanESM5, CNRM-CM6-1, GFDL-CM4, GISS-E2-1-G, HadGEM3-GC31-LL, IPSL-CM6A-LR, MIROC6, NorESM2-LM). The time-series of historical ERF is calculated as the difference of net TOA radiative flux between a 30-year control run (*piClim-control*), where all forcing agents are fixed to pre-industrial levels, and a forcing run (*piClim-histall*), where time-varying atmospheric concentrations of all historical forcing agents are imposed. Historical ERF from a single group of forcing agents (e.g., greenhouse gases, anthropogenic aerosols, natural forcings including volcanoes and solar variability) can also be estimated from single-forcing runs of RFMIP (*piClim-histghg*, *piClim-histaer*, *piClim-histnat*, respectively). We also estimate ERF of CO₂ doubling, F_{2x} , from RFMIP *piClim-4xCO2* simulations, where CO₂ is abruptly quadrupled and held constant for 30yrs while SST and SIC fields are fixed. F_{2x} is computed from the TOA radiation changes of the 30yr-average (scaled by 1/2 to estimate the forcing for CO₂ doubling from CO₂ quadrupling simulations). For all RFMIP simulations, the ensemble mean is used when more than one member of the simulation exist.

Note that the TOA radiation flux changes derived from the fixed-SST simulations includes the effect of temperature changes over land and sea ice, which should be considered as part of the radiative response rather than ERF. We remove this portion of radiative effects by subtracting off the global-mean surface air temperature change scaled by each model’s radiative feedback parameter from its *abrupt4xCO2* simulation – the method proposed in Hansen et al. (2005). Recent studies find advantages in several new correction methods, such as fixing both SST and land-surface temperatures in AGCM simulations (Andrews et al., 2021), or using surface temperature radiative kernels (Smith et al., 2020). We choose to apply the Hansen et al. (2005) method here given that it is a widely used method and readily improves ERF estimates using the available output of

the RFMIP simulations. All the historical ERFs are calculated as global and annual means, spanning the period 1850 – 2014 (the same interval of fully-coupled *historical* simulations).

2.2 Historical simulations of AOGCMs and AGCMs

Within *historical* simulations of AOGCMs, we compute global mean N and T from the mean of all available ensemble members, in attempt to reduce noises from internal variability. Except for GFDL-CM4 (1 member), NorESM2-LM (3 members), and HadGEM3-GC31-LL (4 members), all models have more than 10 *historical* ensemble members available. The annual mean changes of N and T relative to pre-industrial levels are calculated by subtracting a linear fit of the global annual mean *piControl* values to remove unforced model drift. Note that ΔN , ΔF , and ΔT in the energy budget framework (Eq. 1) can also be defined as differences between two specific historical states. We will elaborate the periods over which we compute the historical energy balance in the following two sections. In order to examine the contributions of individual forcing agents to historical climate change, we also employ single-forcing historical simulations (*hist-GHG*, *hist-aer*, *hist-nat*) described by the Detection and Attribution Model Intercomparison Project (DAMIP; Gillett et al., 2016), where only one type of forcing agent is changed while all other forcing agents are fixed at preindustrial levels.

Results from the coupled AOGCMs are compared to two sets of AGCM simulations. One is the *amip* simulation, a CMIP6 DECK experiment (Eyring et al., 2016) where AGCMs are forced by time-evolving observed SST and SIC fields and by time-varying historical forcing agents. While *amip* simulations are available for all of the 8 CMIP6 models assessed here, they are performed only over 1979 – 2015. To investigate early historical energy budget in AGCMs, we also make use of *amip-piForcing* simulations described by the Cloud Feedback Model Intercomparison Project (CFMIP; Webb et al., 2017), which are available from 1870 to 2014. Similar to *amip*, the *amip-piForcing* simulations are forced by observed SST and SIC fields while all forcing agents are fixed at pre-industrial levels (i.e., ERF is zero). Radiative feedbacks are in theory identical between a model’s *amip-piForcing* and *amip* runs because SST and SIC fields are the same, assuming the linearity of the global energy balance (Eq. 1) and that the ERF added to *amip* simulations are accurately quantified by RFMIP simulations. A caveat is that only 6 out of 8 models used here (CanESM5, CNRM-CM6-1, GFDL-CM4, HadGEM3-GC31-LL, IPSL-CM6A-LR, MIROC6) have *amip-piForcing* experiments available. Given that most of the variability in TOA radiative fluxes comes

about through variations in SSTs which are fixed in AGCM simulations, for both sets of AGCM simulations we only use the first realization of each model.

3 Historical Energy Budget Constraints on Radiative Feedbacks and EffCS

In the energy budget framework, $\text{EffCS}_{\text{his}}$ can be written as:

$$\text{EffCS}_{\text{his}} = -\frac{F_{2x}}{\lambda_{\text{his}}}, \quad (3)$$

where the historical effective radiative feedback parameter (λ_{his}) is given by:

$$\lambda_{\text{his}} = \frac{\Delta N - \Delta F}{\Delta T}. \quad (4)$$

We first show historical variations in λ_{his} , calculated by a linear regression form of Eq. 4 in a sliding 30-year window. We find remarkable differences in decadal-scale radiative feedbacks between *historical* simulations (black line in Fig. 1a) and *amip-piForcing* simulations (blue line in Fig. 1a). While natural variability may have played a dominant role in the first half of the 20th century, where net ERF was relatively small (Fig. S1), the discrepancy between AOGCMs and AGCMs persists throughout the full historical period towards early 21st century. Notably, λ_{his} in the *amip-piForcing* simulations of AGCMs trends toward more-negative values since 1970s to present, consistent with earlier studies using CMIP5 models (Andrews et al., 2018; Silvers et al., 2018; Gregory et al., 2020; Dong et al., 2019); whereas in the *historical* simulations of AOGCMs, the trend of λ_{his} is rather weak or even slightly towards more-positive values. During the second half of the century, λ_{his} values from AOGCMs track those in *hist-GHG* simulations (red line), suggesting the simulated feedbacks are primarily driven by GHG forcing, which has dominated global net ERF over this period (Fig. S1).

We next assess $\text{EffCS}_{\text{his}}$ from energy budget constraints within the *historical* simulations of the AOGCMs and the AGCMs. To compute the energy budget in Eqs. 3 and 4, the time interval over which anomalies (Δ) are calculated needs to be carefully chosen to avoid short-term variability and effects of volcanic eruptions (Lewis and Curry 2014; Forster 2016). Previous studies have often used two methods: (1) taking finite differences between a base period and a final period (Lewis & Curry, 2015, 2018; Winton et al., 2020; Sherwood et al., 2020); or (2) using regression over the full period of interest (Gregory et al., 2020; Andrews et al., 2019). Since we are comparing EffCS between

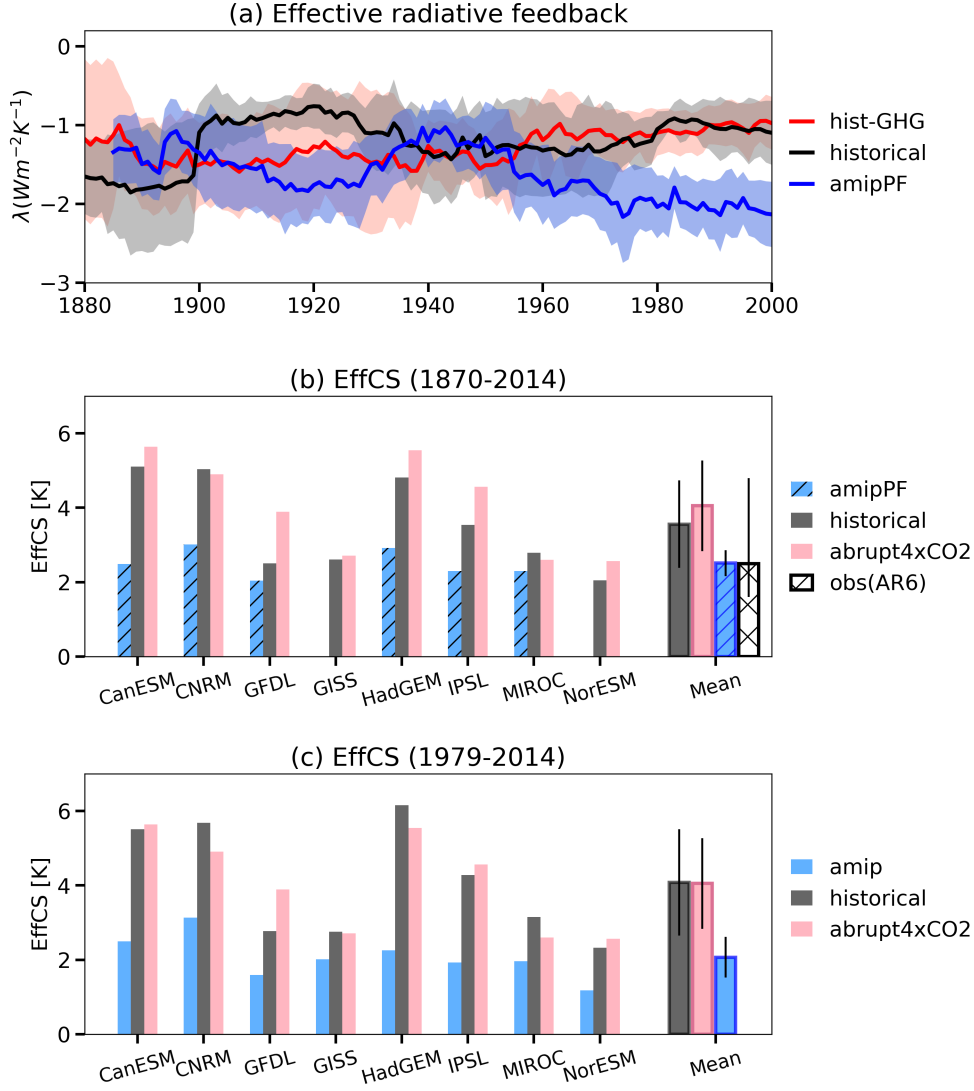


Figure 1. Historical energy budget constraints on net radiative feedback and EffCS. (a) Time series of the estimated historical radiative feedbacks (λ_{his}). Thick lines denote multi-model means, shadings denote one standard deviation across models. (b, c) EffCS estimated from the energy budget of (b) full historical record (1870 – 2014) and (c) recent decades (1979 – 2014). The outlined colored bars on the right in (b, c) denote the multi-model mean values of EffCS from corresponding simulations, with error bars indicating one standard deviation across models. The white hatched bar in (b) denotes the median EffCS_{his} value of 2.5K based on observed energy budget changes reported in IPCC AR6 (Forster et al., in press), with the error bars denoting 5-95% range of 1.6 – 4.8 K. Models listed (from the left to right) are: CanESM5, CNRM-CM6-1, GFDL-CM4, GISS-E2-1-G, HadGEM3-GC31-LL, IPSL-CM6A-LR, MIROC6, NorESM2-LM.

AOGCMs and AGCMs (including *amip* simulations which are only available from 1979 onwards), we choose to use the regression method here. That is, the λ_{his} used to compute $\text{EffCS}_{\text{his}}$ (Eq. 3) is calculated via ordinary least squares (OLS) regression of Eq. 4, over two periods of our interest: the full historical period 1870 – 2014 (Fig. 1b), and the recent decades of the Satellite Era 1979 – 2014 (Fig. 1c).

3.1 $\text{EffCS}_{\text{his}}$ from Long-term Historical Energy Budget (1870 - 2014)

The values of $\text{EffCS}_{\text{his}}$ inferred from long-term energy budget in *historical* simulations are generally lower than $\text{EffCS}_{4\times\text{CO}_2}$ from *abrupt4xCO2* simulations (Fig. 1b). As noted above, the difference between $\text{EffCS}_{\text{his}}$ and $\text{EffCS}_{4\times\text{CO}_2}$ has been documented in a few models. For GFDL-CM4, Winton et al. (2020) found an $\text{EffCS}_{\text{his}}$ of 1.8K and an $\text{EffCS}_{4\times\text{CO}_2}$ of 4K ($\text{EffCS}_{4\times\text{CO}_2} = 5\text{K}$ if using yrs 51-300 of the model’s extended *abrupt4xCO2* simulation). For HadGEM3-GC3.1-LL, Andrews et al. (2019) found an effective $F_{2\times}$ of 3.49 W m^{-2} and a historical feedback of $0.86 \text{ W m}^{-2} \text{ K}^{-1}$ (average of 4 ensembles), implying an $\text{EffCS}_{\text{his}}$ of 4.1K, in contrast to the model’s $\text{EffCS}_{4\times\text{CO}_2}$ of 5.5K. For MPI-ESM1.1, Dessler et al. (2018) found an ensemble-median $\text{EffCS}_{\text{his}}$ of 2.72K, slightly lower than the value of EffCS of 2.93K estimated from a CO_2 doubling simulation. Here we show that, within 6 out of 8 fully-coupled CMIP6 AOGCMs assessed, historical energy budget constraints underestimate $\text{EffCS}_{4\times\text{CO}_2}$ from CO_2 quadrupling, with an average of 12% lower across all models (Table S1). Averaging over all 8 AOGCMs, $\text{EffCS}_{\text{his}}$ is 3.56 K ($\pm 1.17\text{K}$; one standard deviation across models, unless noted elsewhere) and $\text{EffCS}_{4\times\text{CO}_2}$ is 4.05K ($\pm 1.46 \text{ K}$), corresponding to an averaged λ_{his} of $-1.15 \text{ W m}^{-2} \text{ K}^{-1}$ ($\pm 0.37 \text{ W m}^{-2} \text{ K}^{-1}$) and $\lambda_{4\times\text{CO}_2}$ (from the regression of 150yrs *abrupt4xCO2* simulations, data from Zelinka et al. 2020) of $-0.97 \text{ W m}^{-2} \text{ K}^{-1}$ ($\pm 0.34 \text{ W m}^{-2} \text{ K}^{-1}$), respectively. Lower values of $\text{EffCS}_{\text{his}}$ are found in AGCM *amip-piForcing* experiments over the same historical period, with a mean $\text{EffCS}_{\text{his}}$ value of 2.51K ($\pm 0.35\text{K}$) across 6 available models, which is lower than the mean $\text{EffCS}_{4\times\text{CO}_2}$ value of 4.52 K ($\pm 1.04 \text{ K}$) across the same 6 models by 44%. Using the Winton et al. (2020) method, i.e., taking ΔN , ΔT and ΔF as differences between 1869 – 1882 and 1995 – 2014, yields nearly the same result (the difference between the two methods is statistically insignificant in a T-test): the mean value of $\text{EffCS}_{\text{his}}$ is 3.50 K ($\pm 1.31 \text{ K}$) from *historical* simulations across all 8 AOGCMs and 2.54 K ($\pm 0.4 \text{ K}$) from *amip-piForcing* simulations across 6 available AGCMs.

The EffCS and radiative feedback differences between historical energy budget constraints and CO₂ quadrupling in models arise primarily from differences between historical and near-equilibrium warming patterns (Fig. 2). Under CO₂ quadrupling, AOGCMs generally project a warming pattern that is representative of the equilibrium response showing polar amplification and weakened tropical Pacific west-east SST gradient (Fig. 2c; Andrews et al., 2015; Ceppi & Gregory, 2017; Andrews & Webb, 2018; Dong et al., 2020); whereas the SST trend pattern in *historical* simulations appears to be more spatially uniform (Fig. 2a). It has been argued that the projected enhancement of warming in the tropical eastern Pacific relative to the tropical western Pacific in models tends to weaken the lower tropospheric stability, thereby weakening the negative low cloud feedback and negative lapse-rate feedback, producing a higher EffCS (Zhou et al., 2016; Ceppi & Gregory, 2017; Andrews & Webb, 2018; Dong et al., 2019). In contrast, the relatively uniform tropical warming patterns simulated in *historical* simulations would maintain negative cloud feedback and therefore lower EffCS. The fact that EffCS_{his} estimates from *amip-piForcing* simulations are even lower reflects that the observed historical warming pattern shows slightly enhanced warming in the Indo-Pacific Ocean and delayed warming in both the eastern Pacific Ocean and part of the Southern Ocean (e.g., Zhou et al., 2016; Dong et al., 2019, 2020; Silvers et al., 2018).

The historical pattern effect that leads to lower values of EffCS_{his} may partially result from various non-CO₂ forcing agents that have operated in the historical period (e.g., Marvel et al., 2016; Forster, 2016). Gregory et al. (2020) suggest that volcanic forcing may bias estimate of EffCS from CO₂ quadrupling by causing different surface warming patterns in CMIP5 models. Winton et al. (2020) find that a large portion of the EffCS_{his} underestimate in GFDL-CM4 is attributable to its large efficacy of aerosol forcing. To test this possibility within other CMIP6 models, we make use of the DAMIP non-GHG forcing simulations, namely, *hist-aer* and *hist-nat* (Fig. S2). Within all but one model, natural forcing (volcanoes and solar variability) alone produces even lower values of EffCS_{his} than those from *historical* simulations (i.e., a larger historical pattern effect). In comparison, when forced by anthropogenic aerosol forcing alone, four models show a larger historical pattern effect while three models show a reduced pattern effect. These results suggest that natural forcing may be key to the historical pattern effect, while the effect of aerosol forcing is less robust across models.

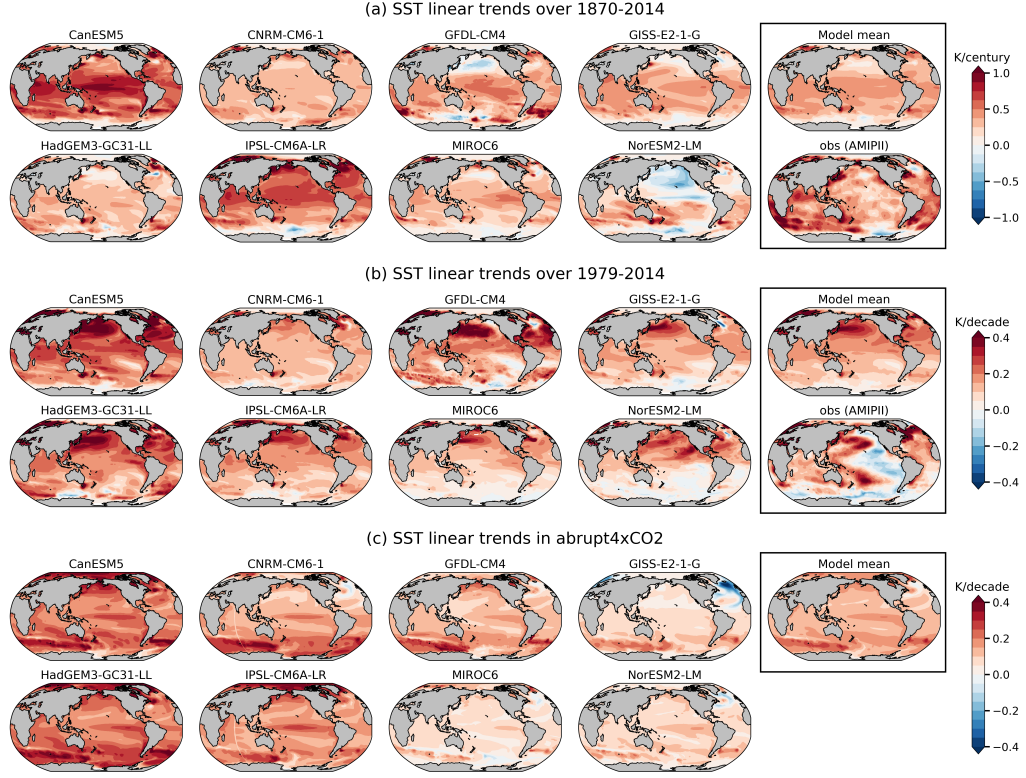


Figure 2. Historical and equilibrium SST trend patterns. SST linear trends over (a) 1870 – 2014, (b) 1979 – 2014, and (c) 150 years of *abrupt4xCO₂* simulations, calculated via OLS regressions of annual-mean SST against time. The observed SST trend patterns in (a, b) are calculated using AMIP-II dataset (Hurrell et al., 2008). The model-mean SST trend patterns in all panels are calculated by averaging over all 8 AOGCMs.

3.2 EffCS_{his} from Recent Energy Budget (1979-2014)

Having quantified the long-term historical energy budget constraint on EffCS, we next focus on the most recent decades 1979 – 2014 (Fig. 1c), where observations of global SSTs have been improved by satellite products. This is also the period where GHG forcing has increased dramatically while aerosol forcing trends are relatively small (Fig. S1). With stronger ERF having operated over this period, nearly all coupled AOGCMs produce higher values of EffCS_{his}, with a multi-model mean EffCS_{his} of 4.08K (corresponding to a mean radiative feedback of $-1.02 \text{ W m}^{-2} \text{ K}^{-1}$), comparable to the mean EffCS_{4xCO2} of 4.05K.

Does this imply that the historical pattern effect is weak in recent decades? In fact, the EffCS_{his} values over this period from all 8 AOGCMs are substantially higher than values of EffCS_{his} from their AGCM counterparts driven by observed warming patterns within *amip* simulations (blue bar in Fig. 1c) and *amip-piForcing* simulations (not shown). Averaging over all AGCMs, the mean EffCS_{his} and the corresponding λ_{his} from *amip* experiments is 2.07 K ($\pm 0.57 \text{ K}$) and $-1.92 \text{ W m}^{-2} \text{ K}^{-1}$ ($\pm 0.58 \text{ W m}^{-2} \text{ K}^{-1}$), respectively. The EffCS_{his} difference between coupled AOGCMs and their counterpart AGCMs can be traced to the difference between modeled and observed SST patterns over recent decades. The ensemble-mean SST trend pattern in *historical* simulations of AOGCMs fails to capture many key features in observations (Fig. 2b), including the pronounced cooling trends over the eastern Pacific and Southern Ocean. In particular, the observed enhancement of tropical Pacific zonal SST gradient has been linked to the observed increase in low clouds over the stratocumulus deck, which contributes to a more-negative radiative feedback and lower EffCS (Zhou et al., 2016; Ceppi & Gregory, 2017; Dong et al., 2019; Fueglistaler, 2019). A few studies have argued that the observed tropical Pacific SST pattern may be driven by anthropogenic sulfate aerosol forcing (Takahashi & Watanabe, 2016) or volcanic forcings (Gregory et al., 2020). Using the DAMIP simulations, we found that the SST trend patterns driven by anthropogenic aerosol forcing and natural forcing are indeed more spatially heterogeneous, with some models showing weak cooling in the tropical eastern Pacific (Fig. S3). However, the cooling trends produced in these non-GHG simulations are much weaker than that observed, and are therefore generally overwhelmed by the warming trends produced by GHG forcing (Fig. S3a).

It is also possible that the observed warming pattern is in part a result of natural variability and therefore expected to differ from the ensemble mean of model simulations. For example, Watanabe et al. (2021) found that the observed equatorial Pacific west-east SST gradient over a longer historical period (1951-2010) lies within the range of large ensembles of model simulations. Olonscheck et al. (2020) also suggests a general consistency between observed SSTs and those simulated by CMIP5 and CMIP6 models, when focusing on specific regions. However, such regional analyses may be insufficient to explain the broad pattern of observed SST trends beyond the equatorial Pacific (e.g., the cooling off the coast in the subtropics and in the Southern Ocean), and their results may be sensitive to the region and time interval selected. We have examined $\text{EffCS}_{\text{his}}$ and the equatorial Pacific zonal SST gradient for all individual members of *historical* simulations. We define the zonal SST gradient following Watanabe et al. (2021): the difference between the eastern Pacific (180°- 80°W, 5°S - 5°N) and the western Pacific (110°E-180°, 5°S - 5°N). But we calculate SST linear trends over 1979 – 2014 instead of 1951 – 2010 as in Watanabe et al. (2021). Over these recent decades, nearly all of the 180 CMIP6 ensemble members fail to capture the low $\text{EffCS}_{\text{his}}$ values from the corresponding *amip* simulations and the observed zonal SST gradient (Fig. S4), suggesting a significant bias in the pattern effect between AOGCMs and observations.

Identifying the causes of the recent observed SST trend pattern is beyond the scope of this study. Our results on the historical energy budget constraints suggest that $\text{EffCS}_{\text{his}}$ estimates from *historical* simulations generally underestimate $\text{EffCS}_{4\times\text{CO}_2}$ from CO₂ quadrupling due to the pattern effect. However, the historical pattern effect is relatively small over recent decades in AOGCMs, owing to the fact that their historical warming patterns over recent decades are not substantially different from their equilibrium warming patterns. In section 5, we will further examine model-observation comparisons.

4 Historical Energy Budget Constraints on TCR

In the energy budget framework, TCR can be inferred from sufficiently long-term historical record where ΔT increases approximately proportional to ΔF :

$$\text{TCR}_{\text{his}} = \Delta T \frac{F_{2\times}}{\Delta F}. \quad (5)$$

Under the global energy framework (Eq. 1), TCR_{his} is governed by both historical radiative feedback (λ_{his}) and ocean heat uptake (OHU) efficiency (κ_{his}), with the relation-

ship between these approximated as (Gregory & Mitchell, 1997; Raper et al., 2002; Gregory & Forster, 2008; Gregory et al., 2015):

$$\text{TCR}_{\text{his}} = \frac{F_{2x}}{\kappa_{\text{his}} - \lambda_{\text{his}}}, \quad (6)$$

where κ_{his} is defined as:

$$\kappa_{\text{his}} = \frac{\Delta N}{\Delta T}. \quad (7)$$

Here we calculate TCR_{his} from *historical* simulations using Eq. 5, where anomalies (Δ) are averaged over 1995 – 2014 relative to 1869 – 1882. This period is chosen to cover a sufficiently long time of historical record, and also to be largely consistent with several recent studies (Lewis & Curry, 2018; Winton et al., 2020). As noted above, Winton et al. (2020) found a TCR_{his} of 1.27K for GFDL-CM4, lower than the model’s $\text{TCR}_{1\text{pct}}$ of 2.05K. Here we find that most of the AOGCMs are consistent with GFDL-CM4 – the historical energy budget constraint underestimates TCR values from *1pctCO2* simulations, by about 12% on average (Fig. 3a). The mean TCR_{his} value across 8 AOGCMs is 1.84K ($\pm 0.51\text{K}$), lower than the mean $\text{TCR}_{1\text{pct}}$ value of 2.08K ($\pm 0.43\text{K}$).

As shown in Eq. 6, the difference between TCR_{his} and $\text{TCR}_{1\text{pct}}$ could arise from changes in radiative feedbacks and/or changes in OHU efficiency over time (Gregory et al., 2015). To separate these two factors, we estimate λ and κ from *historical* and *1pctCO2* simulations, following Eq. 4 and Eq. 7, respectively. For *historical* estimates, ΔN , ΔT and ΔF are taken as finite differences between 1995 - 2014 and 1869 - 1882. For *1pctCO2* estimates, ΔN and ΔT are from the 20-year period centered on year 70 of the simulation when CO_2 is doubled (ΔT is equivalent to $\text{TCR}_{1\text{pct}}$); ΔF at the time of CO_2 doubling is approximated by F_{2x} , with a caveat that the true F_{2x} in *1pctCO2* simulations was found slightly non-logarithmic (Gregory et al., 2015, 2020). In all models κ_{his} is larger than $\kappa_{1\text{pct}}$ which could contribute to the lower values of TCR_{his} relative to $\text{TCR}_{1\text{pct}}$ (Fig. 3b). A weakening of κ over time has also been discovered within *1pctCO2* simulations, from the first doubling of CO_2 to the second doubling, which contributes to an increase in TCR during the second 70-yr of the simulations (e.g., Gregory & Forster, 2008; Gregory et al., 2015). On the other hand, the difference between λ_{his} and $\lambda_{1\text{pct}}$ varies by models (Fig. 3c). Two models show λ_{his} more negative than $\lambda_{1\text{pct}}$, along with their large κ_{his} , suggesting that the lower values of TCR_{his} in these models are owing to changes in both radiative feedbacks and OHU efficiency. The rest of the models show λ_{his} either very close to or slightly less negative than $\lambda_{1\text{pct}}$, suggesting a dominant role of changes in κ . One

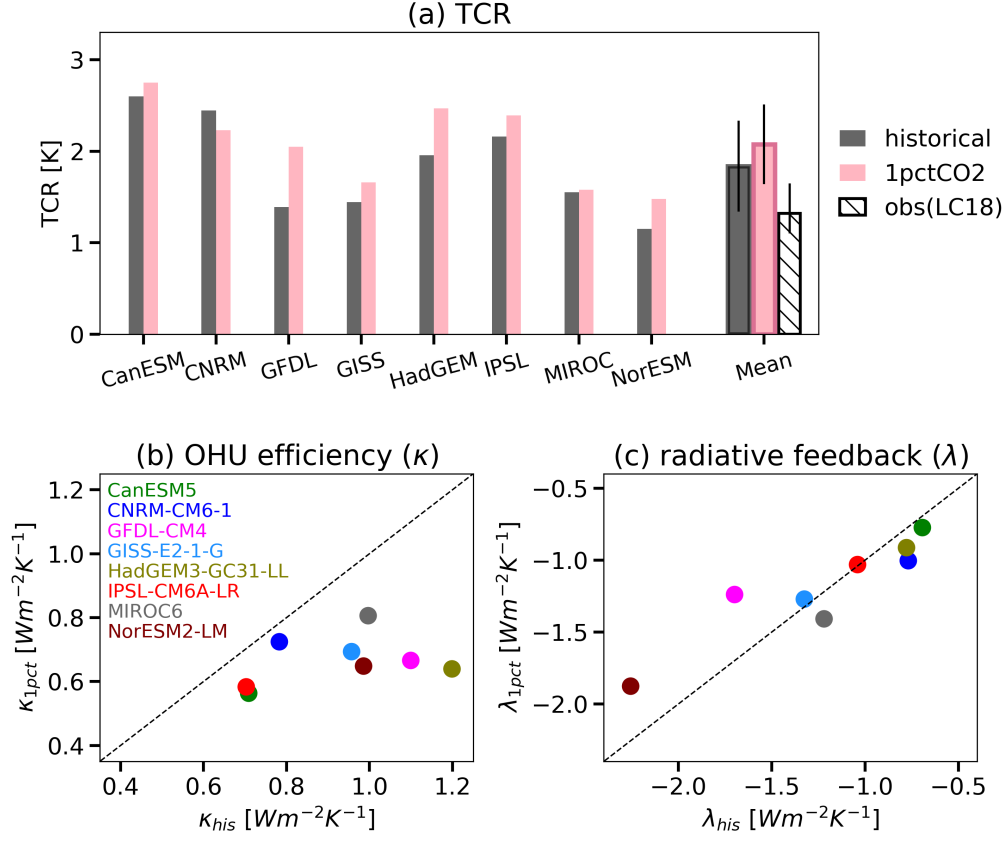


Figure 3. (a) TCR estimates from historical energy budget constraints and *1pctCO2* simulations. Black bars denote TCR_{his} values from fully-coupled *historical* simulations. Red bars denote TCR_{1pct} values from *1pctCO2* simulations. The white hatched bar denotes the best estimate of TCR_{his} of 1.32K based on observed energy budget changes reported by Lewis and Curry (2018), with a 17-83% range of 1.1-1.65K. (b) Ocean heat uptake efficiency and (c) radiative feedback from *historical* and *1pctCO2* simulations of all 8 AOGCMs.

exception is CNRM-CM6-1, whose TCR_{his} is higher than $\text{TCR}_{1\text{pct}}$. The overestimate of its TCR_{his} can be traced to a less-negative λ_{his} and a small difference in κ_{his} .

In summary, we find an overall underestimate of TCR of about 0.2K using historical energy budget constraints within AOGCMs. Values of TCR_{his} are generally biased low owing to the combination of too-negative radiative feedback and/or too-large OHU efficiency during the historical period. The differences in λ and κ between *historical* and *1pctCO2* are largely ameliorated when using *hist-GHG* simulations (Fig. S5), suggesting that the underestimate of TCR_{his} is mostly driven by historical non-GHG forcings. Overall, these results suggest that as time evolves and CO_2 forcing increases, the weakening of both radiative feedback and OHU efficiency could lead to higher values of TCR than those inferred from historical energy budget constraints.

5 Discussions and Conclusions

In the previous two sections, we have compared estimates of EffCS and TCR between different simulations of coupled and atmosphere-only GCMs. How do the model results compare to values of $\text{EffCS}_{\text{his}}$ and TCR_{his} from the observed energy budget constraints, and what implications do the results have for our interpretation of these observation-based estimates?

In Figs. 1 and 3 we show that the reported values of $\text{EffCS}_{\text{his}}$ and TCR_{his} from observations are much lower than the values of $\text{EffCS}_{4\times\text{CO}_2}$ and $\text{TCR}_{1\text{pct}}$ from CMIP6 models. For an observation-based estimate of $\text{EffCS}_{\text{his}}$, we use values reported in IPCC AR6 (Forster et al., in press): a median value of 2.5K and 5 - 95% range of 1.6 – 4.8K based on observed energy budget changes from 1850 - 1900 to 2006 – 2019 (Fig. 1b). For TCR, we use values reported by Lewis and Curry (2018): a median value of 1.32K and a 17–83% range of 1.1 – 1.65 K based on observed energy budget changes over 1869 – 1882 to 1995 – 2016 (Fig. 3). Values of $\text{EffCS}_{\text{his}}$ from AGCM simulations forced by observed SST patterns are well in line with observation-based values of $\text{EffCS}_{\text{his}}$ (c.f. blue bars and white bar in Fig. 1b), despite the fact that AOGCM values of $\text{EffCS}_{\text{his}}$ and $\text{EffCS}_{4\times\text{CO}_2}$ are both higher, confirming the fidelity of the radiative response of atmospheric models given observed SST and SIC trends (Andrews et al., 2018; Loeb et al., 2020). The difference between projected $\text{EffCS}_{4\times\text{CO}_2}$ and observationally-constrained $\text{EffCS}_{\text{his}}$ is thus owing to changes in SST patterns with time. It implies that if nature evolves towards

equilibrium in the way that AOGCMs project, we should expect higher values of EffCS and TCR (i.e., evolving toward $\text{EffCS}_{4\times\text{CO}_2}$ and $\text{TCR}_{1\text{pct}}$) in the future than those inferred from observed historical energy budget constraints.

Our findings are broadly consistent with earlier studies focusing on two individual CMIP6 models (Andrews et al., 2019; Winton et al., 2020): historical energy budget constraints generally (within 6 out of 8 AOGCMs) underestimate the values of EffCS from CO_2 quadrupling and TCR from CO_2 ramping, both by 12% on average. The underestimate of $\text{EffCS}_{\text{his}}$ is owing to differences in radiative feedbacks induced by the pattern effect; the underestimate of TCR_{his} is owing to a combination of differences in both radiative feedbacks and ocean heat uptake efficiency. Using observations, historical energy budget constraints provide even lower values of $\text{EffCS}_{\text{his}}$ and TCR_{his} , which are in line with the values from AGCMs forced by observed SSTs and SICs. Accounting the pattern effect and assuming the observed SST pattern will evolve towards the projected equilibrium warming pattern, the observed historical energy budget may provide a biased-low constraint on EffCS and TCR.

That said, the projections by GCMs are confronted by not only uncertainties associated with atmospheric physics, e.g., cloud feedbacks (Webb et al., 2013; Zelinka et al., 2020; Sherwood et al., 2020), but also a critical open question: how reliable are model projections of future SST and SIC patterns? We find that estimates of $\text{EffCS}_{\text{his}}$ and TCR_{his} from *historical* simulations of coupled AOGCMs fall outside of the range of observation-based values, due to differences between observed and modeled SST trend patterns, which are particularly acute over recent decades. If the observed SST trend pattern (e.g., the strengthening of the tropical zonal SST gradient) is caused by internal natural variability, which will reverse sign in the coming decades according to AOGCM projections (Watanabe et al., 2021), then the higher values of EffCS and TCR found within AOGCMs may be more informative about near-future climate change under continued CO_2 forcing. If the recent observed SST trend pattern is a result of model biases in the response to anthropogenic forcing (e.g., Seager et al., 2019; Coats & Karnauskas, 2017), the lower values of $\text{EffCS}_{\text{his}}$ and TCR_{his} from observations may persist over the coming decades, in which case 21st century warming may be lower than GCMs project. This work suggests that understanding the causes of the recent observed surface warming pattern and model-observation discrepancies is critical for constraining transient and near-equilibrium climate change.

Acknowledgments

We thank Michael Winton and Nadir Jeevanjee for constructive comments. YD, KCA were supported by National Science Foundation Grant AGS-1752796. CP was supported by National Science Foundation grant OCE-2002385. DSB was supported by the Tamaki Foundation. TA was supported by the Met Office Hadley Centre Climate Programme funded by BEIS and Defra, and the European Union’s Horizon 2020 research and innovation program under grant agreement No. 820829 (CONSTRAIN project). Funding for PMF was provided by the European Union’s Horizon 2020 Research and Innovation Programme under grant no. 820829 (CONSTRAIN). CJS was supported by a NERC/IIASA Collaborative Research Fellowship (NE/T009381/1). HS was supported by the Integrated Research Program for Advancing Climate Models (JPMXD0717935457) and Grants-in-Aid for Scientific Research (21H01161) of the Ministry of Education, Culture, Sports, Science and Technology of Japan. The CMIP6 data used in this study are available at: <https://esgf-node.llnl.gov/search/cmip6/>.

References

- Andrews, T., Andrews, M. B., Bodas-Salcedo, A., Jones, G. S., Kuhlbrodt, T., Manners, J., et al. (2019). Forcings, feedbacks, and climate sensitivity in HadGEM3-GC3.1 and UKESM1. *Journal of Advances in Modeling Earth Systems*, 11(12), 4377–4394.
- Andrews, T., Gregory, J. M., Paynter, D., Silvers, L. G., Zhou, C., Mauritsen, T., et al. (2018). Accounting for changing temperature patterns increases historical estimates of climate sensitivity. *Geophysical Research Letters*, 45(16), 8490–8499.
- Andrews, T., Gregory, J. M., & Webb, M. J. (2015). The dependence of radiative forcing and feedback on evolving patterns of surface temperature change in climate models. *Journal of Climate*, 28(4), 1630–1648.
- Andrews, T., Smith, C. J., Myhre, G., Forster, P. M., Chadwick, R., & Ackerley, D. (2021). Effective radiative forcing in a GCM with fixed surface temperatures. *Journal of Geophysical Research: Atmospheres*, 126(4), e2020JD033880.
- Andrews, T., & Webb, M. J. (2018). The dependence of global cloud and lapse rate feedbacks on the spatial structure of tropical Pacific warming. *Journal of Climate*, 31(2), 641–654.

- 455 Armour, K. C. (2017). Energy budget constraints on climate sensitivity in light of
456 inconstant climate feedbacks. *Nature Climate Change*, 7(5), 331–335.
- 457 Armour, K. C., Bitz, C. M., & Roe, G. H. (2013). Time-varying climate sensitivity
458 from regional feedbacks. *Journal of Climate*, 26(13), 4518–4534.
- 459 Bloch-Johnson, J., Pierrehumbert, R. T., & Abbot, D. S. (2015). Feedback temper-
460 ature dependence determines the risk of high warming. *Geophysical Research*
461 *Letters*, 42(12), 4973–4980.
- 462 Bloch-Johnson, J., Rugenstein, M., Stolpe, M. B., Rohrschneider, T., Zheng, Y., &
463 Gregory, J. M. (2021). Climate sensitivity increases under higher CO₂ levels
464 due to feedback temperature dependence. *Geophysical Research Letters*, 48(4),
465 e2020GL089074.
- 466 Caballero, R., & Huber, M. (2013). State-dependent climate sensitivity in past warm
467 climates and its implications for future climate projections. *Proceedings of the*
468 *National Academy of Sciences*, 110(35), 14162–14167.
- 469 Ceppi, P., & Gregory, J. M. (2017). Relationship of tropospheric stability to climate
470 sensitivity and Earth’s observed radiation budget. *Proceedings of the National*
471 *Academy of Sciences*, 114(50), 13126–13131.
- 472 Coats, S., & Karnauskas, K. B. (2017). Are simulated and observed twentieth
473 century tropical Pacific sea surface temperature trends significant relative to
474 internal variability? *Geophysical Research Letters*, 44(19), 9928–9937.
- 475 Dessler, A. E., Mauritsen, T., & Stevens, B. (2018). The influence of internal vari-
476 ability on Earth’s energy balance framework and implications for estimating
477 climate sensitivity. *Atmospheric Chemistry and Physics*, 18(7), 5147–5155.
- 478 Dong, Y., Armour, K. C., Zelinka, M. D., Proistosescu, C., Battisti, D. S., Zhou,
479 C., & Andrews, T. (2020). Intermodel spread in the pattern effect and its
480 contribution to climate sensitivity in CMIP5 and CMIP6 models. *Journal of*
481 *Climate*, 33(18), 7755–7775.
- 482 Dong, Y., Proistosescu, C., Armour, K. C., & Battisti, D. S. (2019). Attribut-
483 ing historical and future evolution of radiative feedbacks to regional warming
484 patterns using a Green’s function approach: The preeminence of the western
485 Pacific. *Journal of Climate*, 32(17), 5471–5491.
- 486 Eyring, V., Bony, S., Meehl, G. A., Senior, C. A., Stevens, B., Stouffer, R. J., &
487 Taylor, K. E. (2016). Overview of the Coupled Model Intercomparison Project

- 488 Phase 6 (CMIP6) experimental design and organization. *Geoscientific Model*
 489 *Development*, 9(5), 1937–1958.
- 490 Forster, P. (2016). Inference of climate sensitivity from analysis of Earth’s energy
 491 budget. *Annual Review of Earth and Planetary Sciences*, 44, 85–106.
- 492 Forster, P., Richardson, T., Maycock, A. C., Smith, C. J., Samset, B. H., Myhre, G.,
 493 et al. (2016). Recommendations for diagnosing effective radiative forcing from
 494 climate models for CMIP6. *Journal of Geophysical Research: Atmospheres*,
 495 121(20), 12–460.
- 496 Forster, P., Storelvmo, T., Amour, K., Collins, W., Dufresne, J., Frame, D., et al.
 497 (in press). The Earth’s energy budget, climate feedbacks, and climate sen-
 498 sitivity. *Climate Change 2021: The Physical Science Basis. Contribution of*
 499 *Working Group I to the Sixth Assessment Report of the Intergovernmental*
 500 *Panel on Climate Change*.
- 501 Fueglistaler, S. (2019). Observational evidence for two modes of coupling between
 502 sea surface temperatures, tropospheric temperature profile, and shortwave
 503 cloud radiative effect in the tropics. *Geophysical Research Letters*, 46(16),
 504 9890–9898.
- 505 Gillett, N. P., Shiogama, H., Funke, B., Hegerl, G., Knutti, R., Matthes, K., et
 506 al. (2016). The Detection and Attribution Model Intercomparison Project
 507 (DAMIP v1. 0) contribution to CMIP6. *Geoscientific Model Development*,
 508 9(10), 3685–3697.
- 509 Gregory, J. M., Andrews, T., Ceppi, P., Mauritsen, T., & Webb, M. (2020). How
 510 accurately can the climate sensitivity to CO₂ be estimated from historical
 511 climate change? *Climate Dynamics*, 54(1), 129–157.
- 512 Gregory, J. M., Andrews, T., & Good, P. (2015). The inconstancy of the transient
 513 climate response parameter under increasing CO₂. *Philosophical Transactions*
 514 *of the Royal Society A: Mathematical, Physical and Engineering Sciences*,
 515 373(2054), 20140417.
- 516 Gregory, J. M., & Forster, P. (2008). Transient climate response estimated from ra-
 517 diative forcing and observed temperature change. *Journal of Geophysical Re-*
 518 *search: Atmospheres*, 113(D23).
- 519 Gregory, J. M., Ingram, W. J., Palmer, M. A., Jones, G. S., Stott, P. A., Thorpe,
 520 R. B., et al. (2004). A new method for diagnosing radiative forcing and cli-

- 521 mate sensitivity. *Geophysical research letters*, *31*(3).
- 522 Gregory, J. M., & Mitchell, J. F. (1997). The climate response to CO₂ of the Hadley
523 Centre coupled AOGCM with and without flux adjustment. *Geophysical Re-*
524 *search Letters*, *24*(15), 1943–1946.
- 525 Gregory, J. M., Stouffer, R., Raper, S., Stott, P., & Rayner, N. (2002). An obser-
526 vationally based estimate of the climate sensitivity. *Journal of climate*, *15*(22),
527 3117–3121.
- 528 Grose, M. R., Gregory, J., Colman, R., & Andrews, T. (2018). What climate sen-
529 sitivity index is most useful for projections? *Geophysical Research Letters*,
530 *45*(3), 1559–1566.
- 531 Hansen, J., Sato, M., Ruedy, R., Nazarenko, L., Lacis, A., Schmidt, G., et al. (2005).
532 Efficacy of climate forcings. *Journal of Geophysical Research: Atmospheres*,
533 *110*(D18).
- 534 Hurrell, J. W., Hack, J. J., Shea, D., Caron, J. M., & Rosinski, J. (2008). A new
535 sea surface temperature and sea ice boundary dataset for the Community
536 Atmosphere Model. *Journal of Climate*, *21*(19), 5145–5153.
- 537 Lewis, N., & Curry, J. A. (2015). The implications for climate sensitivity of AR5
538 forcing and heat uptake estimates. *Climate dynamics*, *45*(3), 1009–1023.
- 539 Lewis, N., & Curry, J. A. (2018). The impact of recent forcing and ocean heat
540 uptake data on estimates of climate sensitivity. *Journal of Climate*, *31*(15),
541 6051–6071.
- 542 Loeb, N. G., Wang, H., Allan, R. P., Andrews, T., Armour, K., Cole, J. N., et al.
543 (2020). New generation of climate models track recent unprecedented changes
544 in Earth’s radiation budget observed by CERES. *Geophysical Research Letters*,
545 *47*(5), e2019GL086705.
- 546 Marvel, K., Pincus, R., Schmidt, G. A., & Miller, R. L. (2018). Internal variability
547 and disequilibrium confound estimates of climate sensitivity from observations.
548 *Geophysical Research Letters*, *45*(3), 1595–1601.
- 549 Marvel, K., Schmidt, G. A., Miller, R. L., & Nazarenko, L. S. (2016). Implications
550 for climate sensitivity from the response to individual forcings. *Nature Climate*
551 *Change*, *6*(4), 386–389.
- 552 Myhre, G., Shindell, D., Bréon, F., Collins, W., Fuglestad, J., Huang, J., et al.
553 (2013). Anthropogenic and natural radiative forcing. *Climate Change 2013:*

- 554 *The Physical Science Basis. Contribution of Working Group I to the Sixth As-*
555 *essment Report of the Intergovernmental Panel on Climate Change*, 659–740.
- 556 Olonscheck, D., Rugenstein, M., & Marotzke, J. (2020). Broad consistency between
557 observed and simulated trends in sea surface temperature patterns. *Geophysi-*
558 *cal Research Letters*, 47(10), e2019GL086773.
- 559 Otto, A., Otto, F. E., Boucher, O., Church, J., Hegerl, G., Forster, P. M., et al.
560 (2013). Energy budget constraints on climate response. *Nature Geoscience*,
561 6(6), 415–416.
- 562 Pincus, R., Forster, P. M., & Stevens, B. (2016). The Radiative Forcing Model In-
563 tercomparison Project (RFMIP): experimental protocol for CMIP6. *Geoscientific*
564 *Model Development*, 9(9), 3447–3460.
- 565 Proistosescu, C., & Huybers, P. J. (2017). Slow climate mode reconciles histori-
566 cal and model-based estimates of climate sensitivity. *Science Advances*, 3(7),
567 e1602821.
- 568 Raper, S. C., Gregory, J. M., & Stouffer, R. J. (2002). The role of climate sensitivity
569 and ocean heat uptake on AOGCM transient temperature response. *Journal of*
570 *Climate*, 15(1), 124–130.
- 571 Rugenstein, M., Bloch-Johnson, J., Gregory, J. M., Andrews, T., Mauritsen, T., Li,
572 C., et al. (2020). Equilibrium climate sensitivity estimated by equilibrating
573 climate models. *Geophysical Research Letters*, 47(4), e2019GL083898.
- 574 Seager, R., Cane, M., Henderson, N., Lee, D.-E., Abernathey, R., & Zhang, H.
575 (2019). Strengthening tropical Pacific zonal sea surface temperature gradi-
576 ent consistent with rising greenhouse gases. *Nature Climate Change*, 9(7),
577 517–522.
- 578 Sherwood, S., Webb, M. J., Annan, J. D., Armour, K., Forster, P., Hargreaves, J., et
579 al. (2020). An assessment of Earth’s climate sensitivity using multiple lines of
580 evidence. *Reviews of Geophysics*, 58(4), e2019RG000678.
- 581 Silvers, L. G., Paynter, D., & Zhao, M. (2018). The diversity of cloud responses
582 to twentieth century sea surface temperatures. *Geophysical Research Letters*,
583 45(1), 391–400.
- 584 Smith, C. J., Kramer, R. J., Myhre, G., Alterskjær, K., Collins, W., Sima, A., et
585 al. (2020). Effective radiative forcing and adjustments in CMIP6 models.
586 *Atmospheric Chemistry and Physics*, 20(16), 9591–9618.

- 587 Takahashi, C., & Watanabe, M. (2016). Pacific trade winds accelerated by aerosol
588 forcing over the past two decades. *Nature Climate Change*, 6(8), 768–772.
- 589 Watanabe, M., Dufresne, J.-L., Kosaka, Y., Mauritsen, T., & Tatebe, H. (2021).
590 Enhanced warming constrained by past trends in equatorial Pacific sea surface
591 temperature gradient. *Nature Climate Change*, 11(1), 33–37.
- 592 Webb, M. J., Andrews, T., Bodas-Salcedo, A., Bony, S., Bretherton, C. S., Chad-
593 wick, R., et al. (2017). The Cloud Feedback Model Intercomparison Project
594 (CFMIP) contribution to CMIP6. *Geoscientific Model Development*, 10(1),
595 359–384.
- 596 Webb, M. J., Lambert, F. H., & Gregory, J. M. (2013). Origins of differences in
597 climate sensitivity, forcing and feedback in climate models. *Climate Dynamics*,
598 40(3).
- 599 Winton, M., Adcroft, A., Dunne, J., Held, I., Shevliakova, E., Zhao, M., et al.
600 (2020). Climate sensitivity of GFDL’s CM4.0. *Journal of Advances in Model-
601 ing Earth Systems*, 12(1), e2019MS001838.
- 602 Zelinka, M. D., Myers, T. A., McCoy, D. T., Po-Chedley, S., Caldwell, P. M., Ceppi,
603 P., et al. (2020). Causes of higher climate sensitivity in CMIP6 models. *Geo-
604 physical Research Letters*, 47(1), e2019GL085782.
- 605 Zhou, C., Zelinka, M. D., & Klein, S. A. (2016). Impact of decadal cloud variations
606 on the Earth’s energy budget. *Nature Geoscience*, 9(12), 871–874.